Iraqi Journal of Physics, 2026
https://doi.org/10.30723/ijp.v23i2.1346

Vol. 24, No.1, PP. 109-120
P-ISSN: 2070-4003
E-ISSN: 2664-5548

Preparation of $AlCl_3$:ITO Films Using Sol-Gel Dip Coating Method

Alaa M. Theban[1*] and Falah H. Ali[1]
[1]*Department of Physics, College of Science, University of Baghdad, Baghdad, Iraq*
[*]Corresponding author: alaa.m@csw.uobaghdad.edu.iq

Abstract

This paper used the sol-gel dip-coating method to produce pure indium tin oxide (ITO) and ITO thin films doped with $AlCl_3$ at varying concentrations (50, 100, and 150 wt.%). Precursors such as $InCl_3$ and $SnCl_4$ were used in the synthesis. The synthesized ITO samples underwent thorough characterization using UV-Vis, atomic force microscopy (AFM), X-ray diffraction (XRD), field-emission scanning electron microscopy/energy dispersive X-ray spectroscopy (FE-SEM/EDX), and Fourier transform infrared spectroscopy (FTIR). The XRD analysis revealed a strong peak for the (222) plane, showing that the indium oxide in the thin films is very well-organized. EDX analysis confirmed the presence of elements, including indium (In), oxygen (O), tin (Sn), aluminum (Al), and chlorine (Cl), within the deposited layers. According to the FE-SEM images, the average particle diameters were 45.47nm for pure ITO, 62.48, 42.72, and 35.25 nm for ITO with a 50, 100, and 150wt.% $AlCl_3$ ratio, respectively. The AFM analysis indicated that the pure ITO film had an average particle size of 61 nm. In comparison, the films mixed with $AlCl_3$ at 50, 100, and 150 wt.% ratios had average particle sizes of 17, 21, and 68 nm. In addition, the optical band gap of the ITO was measured at 4.5 eV. For films with $AlCl_3$ at 50, 100, and 150 wt.% ratios, the energy gaps were found to be 1.5, 1.73, and 1.83 eV, respectively. The measured contact angle for the ITO film was 332.57°; those with $AlCl_3$ at 50, 100, and 150% were 65.39°, 85.99°, and 78.12°, respectively.

Article Info.

Keywords:
$AlCl_3$ Films, Sol-Gel Dip Coating method, Indium Tin Oxide (ITO), Optical Properties, Contact Angle.

Article history:
Received: Jul. 14, 2024
Revised: Jan. 06, 2025
Accepted: Jan.22, 2025
Published:Mar.01,2026

1. Introduction

Probably one of the most notable advances in the field of advanced materials science and engineering was the doping of In_2O_3:Sn film by $AlCl_3$ using the sol-gel dip coating technique. Indium Tin Oxide (ITO) is a core material known for its very outstanding combination of a very high electrical conductivity with very high optical transparency, which makes it one of the most widely used materials today in a very large number of modern-day optoelectronic applications [1-7]. The sol-gel dip coating technique is one of the versatile and scalable methods that deposit thin films with exceptional thickness and uniformity control, which is very important to attain optimal performance in most device architectures. ITO thin films are highly degenerative n-type semiconductors, normally exhibiting electrical resistance in the range of 2 and $4x10^4$ Ω.cm [8-14]. Such degeneracy follows from the position of the Fermi level (EF) above the conduction band minimum (EC) which is associated with an extremely high charge carrier density and correspondingly very small values of resistivity. Generally, high conductive ITO sheets often have carrier concentrations ranging between 10^{20} cm^{-3} and 10^{21} cm^{-3}. Besides their excellent electrical properties, ITO films also show magnificent optical properties in terms of the wavelength range, namely, high transparency in the visible and good reflectance in the infrared, in addition to good mechanical properties, such as very good adhesion to substrates and good mechanical strength. Based on this, this paper presents detailed investigations into the associated complexities in the fabrication of $AlCl_3$-doped ITO films through the sol-gel dip coating process [15-20].

In particular, the investigations on the structural and optical aspects under doping concentrations and deposition parameters will be underlined. The additional work for this

project will be entered into the ballooning body of knowledge acting toward perfecting the next generation of ITO-based materials that will power modern electronic and photonic devices.

2. Experimental Work

2.1. Preparation of ITO Thin Films

1.1727 g of $InCl_3$ and 0.1402 g of $SnCl_4$, the precursors for ITO, were individually dissolved in 50 mL of double-distilled water. Afterwards, the ingredients in a 100 mL glass container were mixed with constant shaking for 120 minutes after 30 minutes on a magnetic stirrer. The pH solution was adjusted to nine by gradually adding small quantities of NaOH. To modify the pulling speed on the dip-coater device between 2 and 5 mm/s, the glass slide was submerged in the prepared solution while the resultant liquid participated in the process. In the production process, a drying procedure was performed in an oven at 85°C, and then the material was calcined at 500°C for two hours.

2.2. Preparing ITO and Measuring Contact Angle

Three different amounts of (0.2925, 0.0975 and 0.195g) $AlCl_3$ were separately combined with ten milliliters of ethanol to create the ITO combination. After that, the solutions were left to dissolve on a magnetic shaker at room temperature for thirty minutes. Afterwards, the pure ITO solution and ITO solutions with 50, 100, and 150 wt.% $AlCl_3$ mixing ratios that were obtained from mixing $AlCl_3$ with ten milliliters of ITO. Studies on pure ITO film as well as ITO/$AlCl_3$ ratios 50, 100, and 150 wt.% were performed. This was achieved by repeatedly heating and coating the films. Fig. 1 shows how simple, inexpensive, reliable, and repeatable the dip coating process is. This process involves dipping an object into the mixture to create a wet liquid layer. The thickness and characteristics of the film are influenced by many variables, including temperature, solution composition, withdrawal speed, number of coating cycles, immersion length, and ambient humidity. In our experiment, silica glass substrates were immersed in a 20 mL solution three times. Following each immersion, the substrate was allowed to dry for ten minutes at 80°C. Water droplet behavior on the film surfaces was investigated to study the hydrophilic property of the films using the contact angle equipment shown in Fig. 2. A micro-injector syringe (5µl) was positioned vertically above the sample surface to precisely deposit water droplets. Subsequently, a high-resolution camera equipped with a macro lens captured images of the droplets, which were then analyzed using dedicated analytical software.

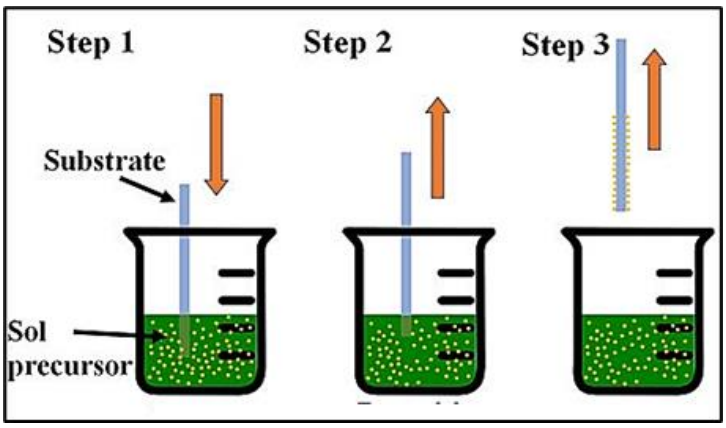

Figure 1: The dip coating method.

Figure 2: Contact angle setup.

3. Results and Discussion

3.1. Optical Studies

The optical qualities were evaluated with a UV-Vis spectrophotometer. Fig. 3(a, b) shows transmission spectra of ITO and $AlCl_3$:ITO with (50, 100, 150 wt.%) mixing ratio in a wavelength range from 250 nm to 1100 nm. The transmittance spectrum of each sample was found to increase with wavelength because the material absorbs less light at longer wavelengths. As the wavelength increases towards the visible and infrared regions, these absorption mechanisms become less significant, allowing lighter to pass through the material. ITO mixed with $AlCl_3$ exhibited lower optical transmittance compared to pure ITO. The observed decrease in transmittance with higher percentages of $AlCl_3$ is due to the increased absorbance caused by the added $AlCl_3$ [21-24]. When $AlCl_3$ is mixed with the material, additional energy levels are introduced between the valence and conduction bands. These new energy levels increase the likelihood of light absorption within the material. Consequently, more light is absorbed and less is transmitted through the material, leading to a decrease in transmittance. The highest values of optical transmission measured for ITO in the infrared region were 29% at ratios of 100 wt.%, 26% at ratios of 150 wt.%, and 30% at ratios of 50 wt.% [25, 26].

In Fig. 4(a,b), the direct optical energy bandgap of ITO and ITO/$AlCl_3$ (50,100,150 wt.%) is presented. The Tauc model found the direct optical energy band gap by looking at where the straight line from the $(\alpha hv)^2$ versus photon energy (hv) graph meets the (hv) axis, as shown in Eq. (1) [27]:

$$\alpha hv = \alpha_o(hv - E_g)^n \quad (1)$$

where, for direct semiconductors, n value is considered 1/2, α stands for the absorption coefficient, v is the light frequency, and E_g represents the material's energy band gap. For pure ITO, the energy band gap was found to be 4.5eV. The energy gaps for ITO/$AlCl_3$ of different mixing ratios 50,100,150wt.% were found to be 1.83, 1.73, and 1.5 eV, respectively. It is observed that the energy gap decreased with the addition of $AlCl_3$. This suggests that the presence of $AlCl_3$ in the samples has introduced some energy levels in the band gap, therefore lowering the energy required by electrons in the valence band to be transferred to the conduction band. This phenomenon is often due to the changes in the electronic structure and composition of the material caused by the addition of $AlCl_3$ [28, 29]. It is also noted that the higher the amount of $AlCl_3$ mixed with ITO, the smaller the energy gap between the valence band and the conduction band.

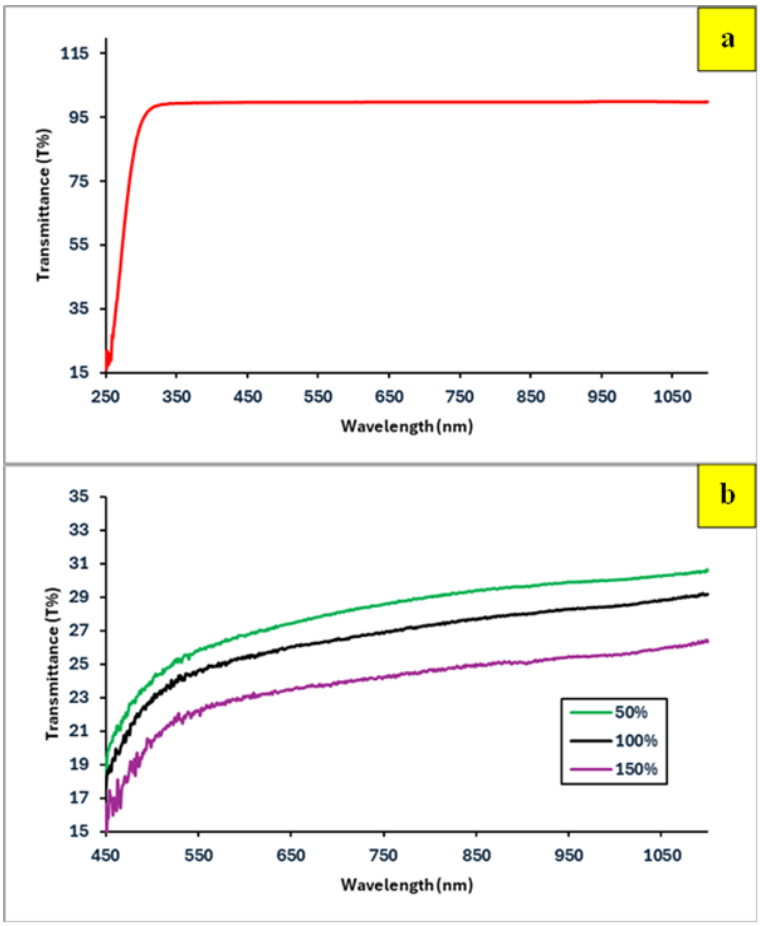

Figure 3: Transmission spectroscopy of (a) pure ITO, and (b) ITO mixed at various ratios 50, 100, and 150 wt% of $AlCl_3$.

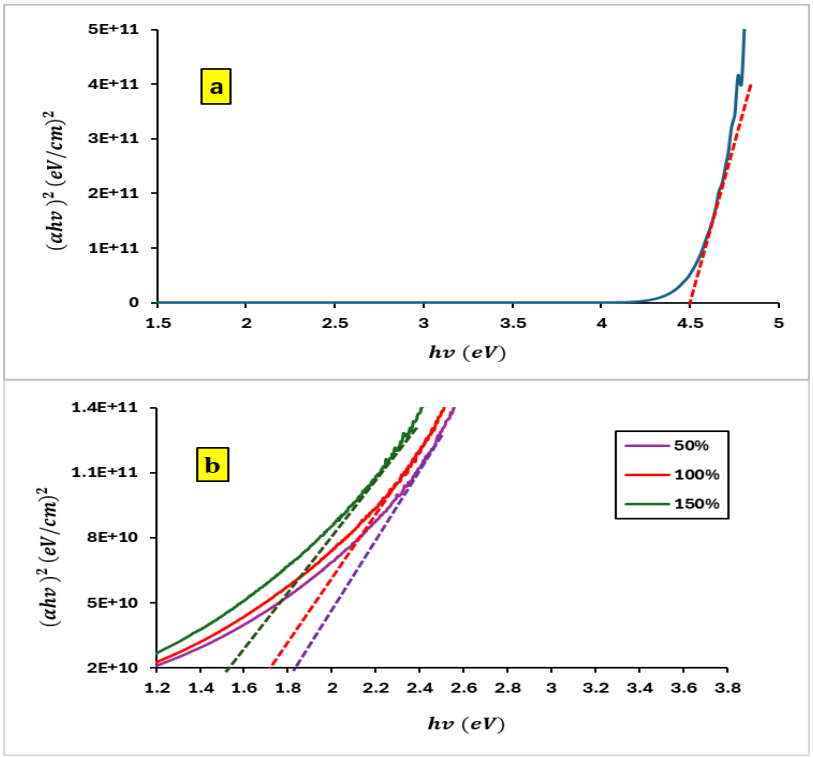

Figure 4: Tauc plots for (a) pure ITO, and (b) ITO mixed at various ratios 50, 100, and 150 wt.% with $AlCl_3$.

Fig. 5(a-d) displays the atomic force microscopy (AFM) images of the pure ITO and ITO/$AlCl_3$ at different ratios 50, 100, and 150wt.%. The dip coating procedure was employed to create these films on a glass substrate. The scanning regions for each image were 5.23×5.23, 2.59×2.59, 2.36×2.36, and 3.75×3.75 μm, respectively. The ITO film exhibits distinct peak distributions, characterized by a particle size of 61 nm and a root mean square height of 10.72 nm. In contrast, the films with varying proportions of $AlCl_3$ 50, 100, and 150 wt.% displayed grains with a distinct convex peak shape and a strong orientation, particularly in the case of the 100 wt.% ratio. The mean diameters of these grains were 17, 21, and 68 nm, respectively. In addition, the root mean square heights of these films were measured to be 1.32, 1.54, and 21.64 nm, respectively. At a high mixing ratio of 150 wt.%, the extra $AlCl_3$ improved the crystalline structure of the material [30, 31]. This enhancement allows the grains to grow larger. The Al atoms likely occupy vacant sites in the crystal lattice, stabilizing the structure and promoting the formation of larger grains. Therefore, a higher mixing ratio results in a more ordered crystalline structure, leading to an increase in grain size [32].

3. 3. X-Ray Diffraction (XRD) Analysis

This study focuses on analyzing structure of pure ITO and ITO/$AlCl_3$ at different ratios 50, 100, and 150 wt.%, using XRD patterns throughout the 2 θ range of 7° to 80°. Fig. 6(a, b) shows the (XRD) patterns of pure and with different mixing ratios samples. The films have a polycrystalline structure, with the most prominent peak at (222), indicating a cubic structure as per JCPDS: 71-2194 [33, 34]. The XRD data demonstrated that the diffusion of aluminum compounds into the samples leads to a drop in intensity at various mixing ratios of 50, 10, and 150 wt.%. This explains the absence of a peak corresponding to aluminum or aluminium oxide. Its absence indicates that aluminum atoms are probably diffusing into the interstitial space within the lattice structure of this ITO. As aluminum atoms occupy these interstitial sites, they disrupt the periodicity of the crystal lattice, leading to a decrease in the intensity of XRD peaks observed at different mixing ratios 50, 100, and 150wt.%. This decrease occurs because aluminum alters the scattering of X-rays within the crystal lattice of ITO, affecting the intensity of diffraction peaks that would otherwise be present in pure ITO. The growth continues to favor the plane (222), with a minor deviation in the 2θ angle. XRD examination verifies the successful synthesis of ITO through the sol-gel process. The Scherrer formula was used to calculate the size of the crystallite (Eq. (2)) [35]:

$$D = \frac{k\lambda}{B\cos\theta} \qquad (2)$$

K should be adjusted to 0.9, λ to 0.154 nm, β is the full width at half-maximum (FWHM), and θ is the Bragg diffraction angle [36]. For ITO samples combined with 50, 100, and 150 wt.%. $AlCl_3$, the average crystallite diameters measured were 44.1, 8.9, 2.6, and 2.5 nm, respectively. The XRD results for each group are summarized in Table 1.

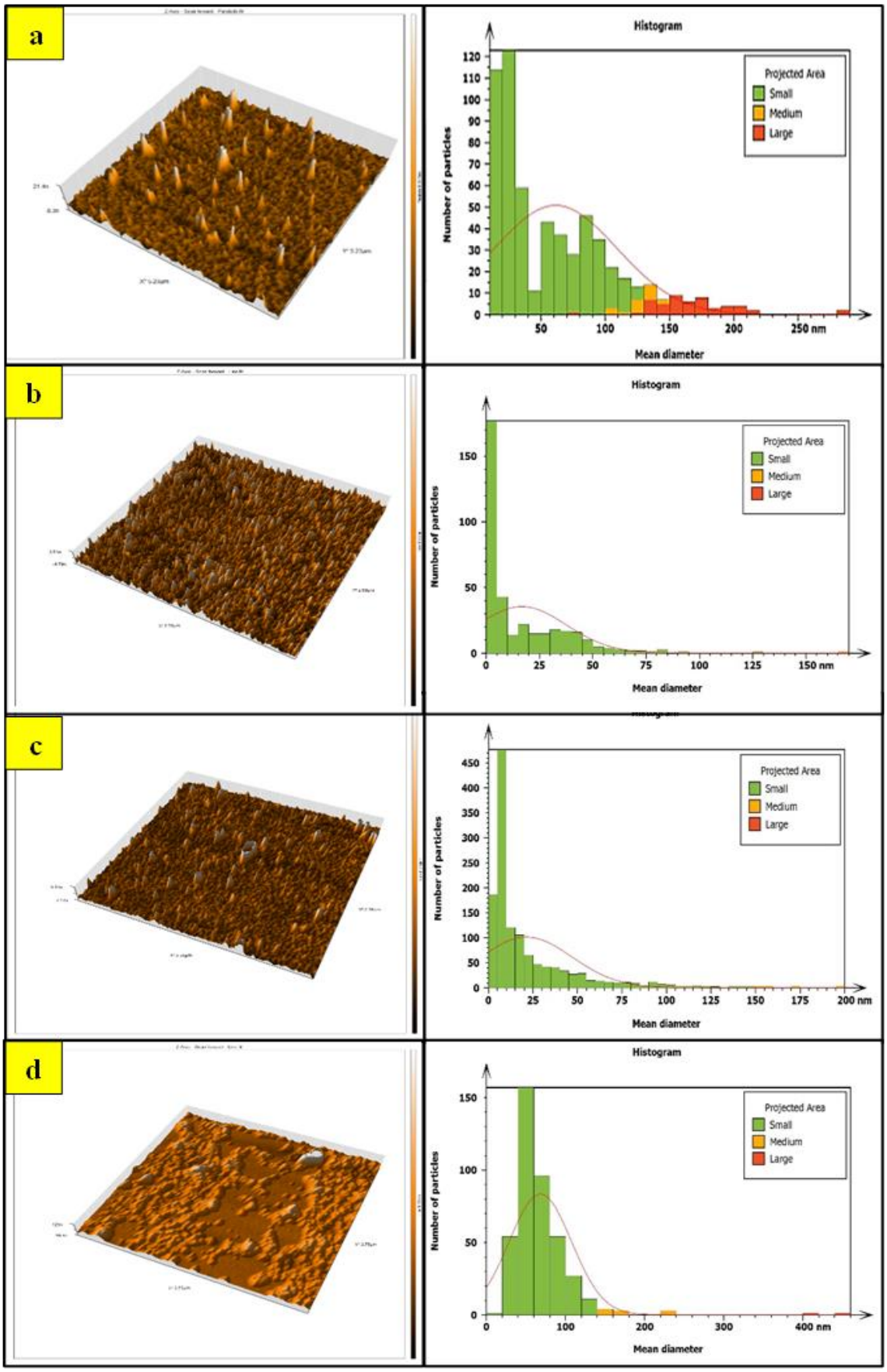

Figure 5: AFM images of the samples: a) the pure film, b) at 50, c) at 100, and d) at 150 wt.%.

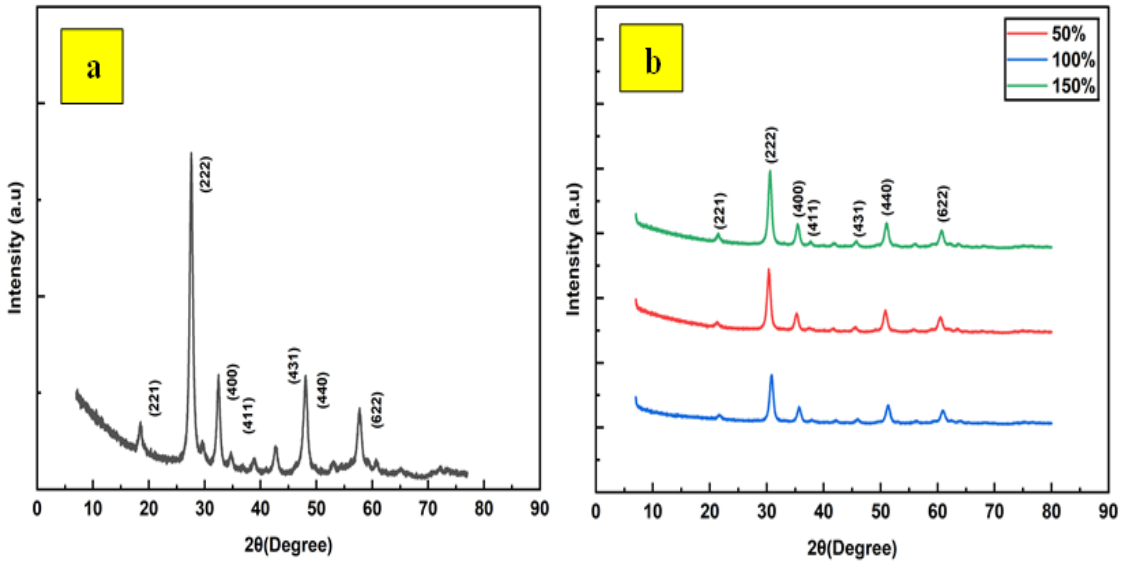

Figure 6: The XRD patterns of a) the pure film, b) at 50, c) at 100, and d) at 150 wt.%.

Table 1: XRD findings summary for all samples.

Sample	2θ (deg)	FWHM (deg)	d(A)	hkl	D (nm)
ITO	21.6	0.10	16.35	(211)	27.0
	30.5	0.30	11.65	(222)	20.6
	35.4	0.20	10.07	(400)	81.0
	37.9	0.20	9.43	(411)	84.1
	45.8	0.20	7.87	(431)	43.2
	51.8	0.20	7.017	(440)	22.0
	60.9	0.30	6.04	(622)	30.7
ITO+$AlCl_3$ 50 wt.%	21.3	0.733	4.17	(211)	4.167
	30.3	0.732	2.94	(222)	2.947
	35.2	0.363	2.55	(400)	2.547
	37.5	0.906	2.39	(411)	46.7
	45.4	0.876	1.99	(431)	2.396
	51.0	0.796	1.79	(440)	1.789
	60.4	0.892	1.53	(622)	1.531
ITO+$AlCl_3$ 100 wt.%	21.7	0.842	4.10	(211)	4.092
	30.8	0.753	2.90	(222)	2.899
	35.7	0.779	2.52	(400)	2.5127
	37.9	0.739	2.37	(411)	2.372
	45.9	0.763	1.98	(431)	1.975
	51.2	0.842	1.78	(440)	2.783
	60.9	0.902	1.52	(622)	1.519
ITO+$AlCl_3$ 150 wt.%	21.5	0.784	4.45	(211)	4.129
	30.5	0.708	2.93	(222)	2.929
	35.4	0.751	2.53	(400)	2.533
	37.6	0.738	2.39	(411)	2.389
	45.6	0.826	1.99	(431)	1.988
	50.9	0.828	1.79	(440)	1.792
	60.6	0.862	1.53	(622)	1.527

The extreme sensitivity of XRD to internal stresses that alter the peak width may be the cause of the discrepancy between AFM and XRD results.

3.4. Energy Dispersive X-ray (EDX) Analysis

EDX is used to examine the composition of samples. Fig. 7 (a-d) illustrates the EDX spectra onto the prepared thin films for pure ITO and ITO/$AlCl_3$ of different mixing ratios (50, 100, and 150 wt%). The deposited coatings composed of elements O, In, Sn, Al, and Cl reveal a remarkable increase in oxygen content on the surface from these spectra. Table 2 displays the atomic percentages and weight values of the pure ITO and ITO mixed with $AlCl_3$ films at 50, 100, and 150 wt.%. EDX analysis confirmed the presence of aluminum (Al) atoms in the structure of the ITO film. However, there were no characteristic peaks related to aluminum or its oxide compounds in the XRD pattern. This may indicate that the aluminum atoms are uniformly distributed inside the crystal lattice of the ITO film. The absence of any discrete peaks for Al in the XRD pattern may further be considered as evidence of the fact that the Al atoms are incorporated or mixed in with the ITO structure and do not form separate crystalline phases of aluminum or aluminum oxide. This, therefore, can diffuse into the material to change whatever properties of the material in question, for instance, its crystallinity and conductivity by modifying the lattice structure of the ITO film.

Figure 7: EDX results for a) Pure ITO film, b) 50, c) 100, d) 150 wt.% $AlCl_3$ mixing ratio.

Table 2: EDX findings summary for all samples.

Sample	element	Atomic%	Weight%
ITO	O	96.9	81.1
	In	1.3	7.9
	Sn	1.8	11.0
ITO+$AlCl_3$ 50 wt.%	O	89.0	69.1
	Al	7.3	9.5
	Cl	0.0	0.0
	In	1.7	9.3
	Sn	2.1	12.1
ITO+$AlCl_3$ 100 wt.%	O	87.7	69.8
	Cl	9.2	12.3
	Fe	0.2	0.3
	In	1.2	6.9
	Sn	1.8	10.7
ITO+$AlCl_3$ 150 wt.%	O	87.6	70.9
	Cl	9.4	12.8
	Fe	0.4	0.7
	In	1.0	5.7
	Sn	1.7	9.9

3. 5. FE-SEM Analysis

The field emission scanning electron microscope scans a sample's surface in a raster pattern using a high-energy electron beam. The procedure parameters of the deposition of thin films affect the surface morphology, which can significantly impact the mechanical, electrical, and optical properties of the film. The SEM images of pure ITO and ITO/$AlCl_3$ thin films of different mixing ratios (50, 100, and 150 wt.%) are shown in Fig. 8(a–d). The pristine film's particles vary in size and form, as seen in Fig. 8(a), with an average diameter of 62.48 nm, becoming cube-shaped. However, a small number of agglomerates have a size of many micrometers. All the ITO films exhibitted almost the same surface morphology at different mixing ratios of $AlCl_3$ (50, 100, and 150 wt.%). These particles were uniformly formed and devoid of cavities and fractures. These characteristics include a larger effective surface area, reduced grain boundaries, enhanced electrical conductivity, and improved optical transmittance due to this uniformity. Across the samples, the average particle size is 45.47, 42.72, and 35.25 nm, for 50, 100, 150 wt.% of $AlCl_3$ mixing ratios with ITO, respectively. There is also agreement on the results with previous literature [37].

3.6. Contact Angle

The contact angle is the angle formed between the tangent to the liquid surface and the solid surface. The contact angle can be large or small depending on the physical properties of the material under study. Fig. 9(a–d) shows the water contact angles measured on ITO and ITO/$AlCl_3$ (50, 100, and 150 wt.%). Among the films analyzed, the contact angle of the pure ITO sample was the smallest, less than 33°. In detail, the contact angles measured were 32.57°, 65.39°, 85.99°, and 78.12° for the pure, 50, 100, and 150 wt.% $AlCl_3$ mixing ratio films, respectively. The surface of the pure ITO film was completely wetted by water. This observation suggests a link between the film's catalytic activity and its hydrophilicity, where lower contact angles indicate greater hydrophilicity. This phenomenon implies that the reduced surface roughness at lower $AlCl_3$ mixing ratios influences the hydrophilic nature of the ITO surface [38, 39].

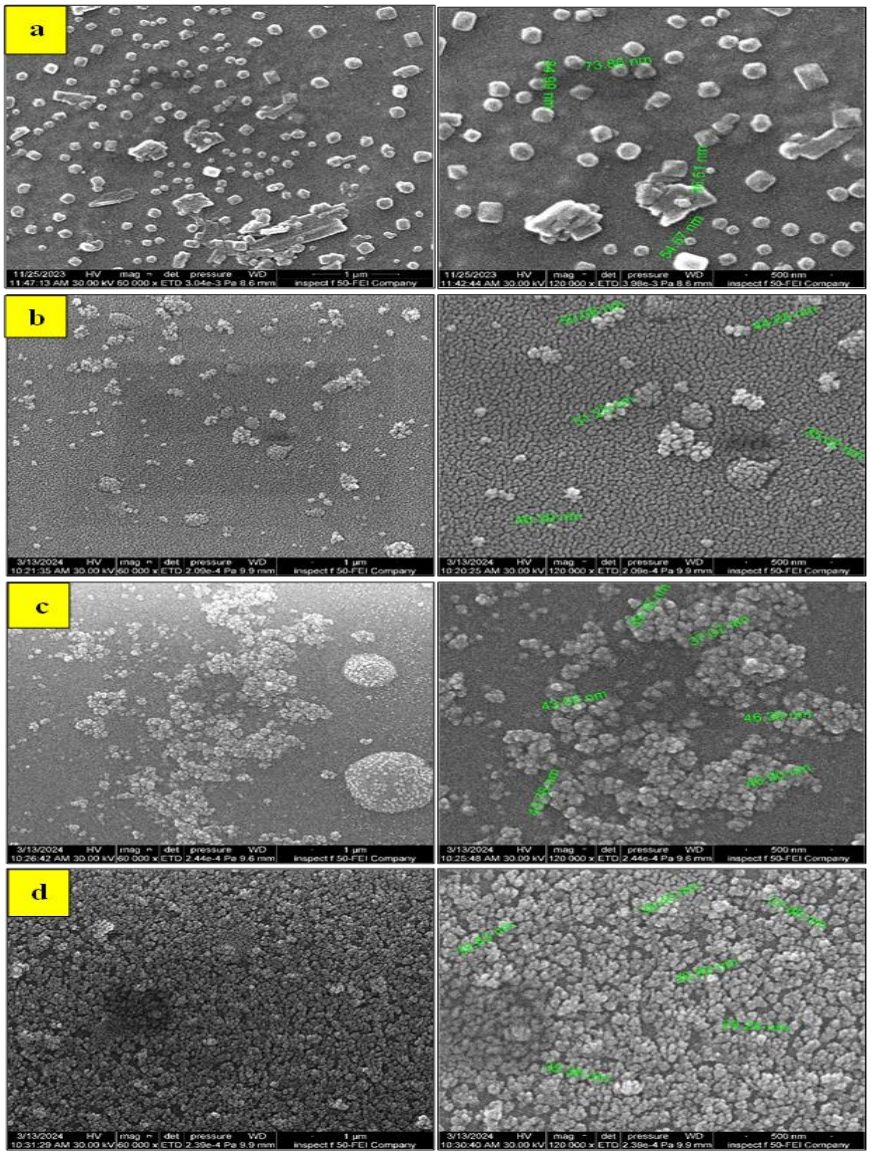

Figure 8: FE-SEM images of the samples: a) Pure ITO film, b) 50, c) 100, d) 150 wt.% of $AlCl_3$.

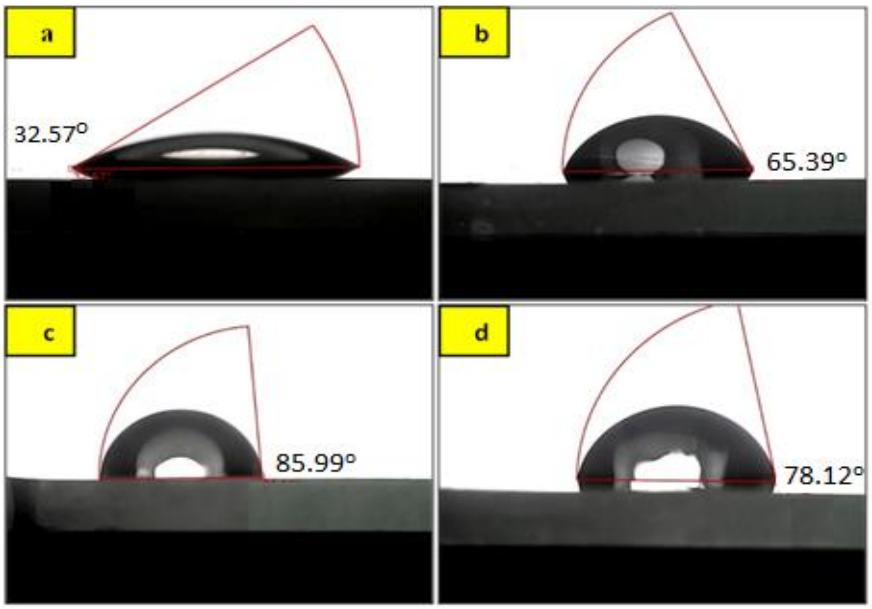

Figure 9: Water droplet on the surface of the samples: a) Pure ITO film, b) 50, c) 100, d) 150 wt.% of $AlCl_3$.

4. Conclusions

This work successfully demonstrated the preparation of $AlCl_3$ (aluminium chloride) films via the sol-gel dip-coating method. This method effectively incorporates $AlCl_3$ into the ITO matrix, thereby altering the film's properties as the mixing ratio varies. The films showed similar surface textures and better electrical conductivity and light transmission, making them suitable for use in optoelectronics, solar cells, and other clear electrode technologies. The sol-gel approach proved reliable for producing homogeneous and high-quality thin films, offering promise for scalable manufacturing processes in related industries.

Conflict of Interest

The authors declare no conflict of interest.

References

1. E. Fanelli, Ph.D Thesis, University of Naples Federico II, Italy, 2013.
2. T. Prabhakar, M.Sc Thesis, The University of Toledo, Ohio, 2013.
3. A. J. Bierbaum, Ph.D Thesis, University of Minnesota, Minnesota, 2013.
4. Y. Ren, P. Liu, R. Liu, Y. Wang, Y. Wei, L. Jin, and G. Zhao, J. All. Comp. **893**, 162304 (2022). https://doi.org/10.1016/j.jallcom.2021.162304.
5. S. A. Bashar, Ph.D Thesis, University of London, England, 1998.
6. H. Liu, V. Avrutin, N. Izyumskaya, Ü. Özgür, and H. Morkoç, Superlatt. Microstruct. **48**, 458 (2010). https://doi.org/10.1016/j.spmi.2010.08.011.
7. G. K. Dalapati, H. Sharma, A. Guchhait, N. Chakrabarty, P. Bamola, Q. Liu, G. Saianand, A. M. S. Krishna, S. Mukhopadhyay, and A. Dey, J. Mat. Chem. A **9**, 16621 (2021). https://doi.org/10.1039/D1TA01291F.
8. R. A. Afre, N. Sharma, M. Sharon, and M. Sharon, Rev. Adv. Mater. Sci. **53**, 79 (2018). https://doi.org/10.1515/rams-2018-0006.
9. S. Y. Khalaf and F. H. Ali, Iraqi J. Phys. **19**, 62 (2021). https://doi.org/10.30723/ijp.v19i49.646.
10. H. D. Hamadalla and F. H. Ali, Iraqi J. Phys. **22**, 57 (2024). https://doi.org/10.30723/ijp.v22i2.1167.
11. Y. Li, Ph.D Thesis, University of Florida, Florida, 2006.
12. R. K. Willardson and A. C. Beer, *Semiconductors and Semimetals* (New York, USA, Elsevier, 1970), p.15.
13. R. K. Jamal, F. H. Ali, M. M. Hameed, and K. A. Aadim, Iraqi J. Sci. **61**, 1032 (2020). https://doi.org/10.24996/ijs.2020.61.5.12.
14. R. K. Jamal, F. H. Ali, and F. A.-H. Mutlak, Iraqi J. Sci. **62**, 2213 (2021). https://doi.org/10.24996/ijs.2021.62.7.11.
15. C.-H. Ho, C.-H. Chan, L.-C. Tien, and Y.-S. Huang, J. Phys. Chem. C **115**, 25088 (2011). https://doi.org/10.1021/jp208789t.
16. A. Fahrenbruch and R. Bube, *Fundamentals of Solar Cells: Photovoltaic Solar Energy Conversion* (New York, Academic Press, 2012).
17. Y. Demirhan, H. Koseoglu, F. Turkoglu, Z. Uyanik, M. Ozdemir, G. Aygun, and L. Ozyuzer, Renew. Ener. **146**, 1549 (2020). https://doi.org/10.1016/j.renene.2019.07.038.
18. A. Luque and S. Hegedus, *Handbook of Photovoltaic Science and Engineering* (UK, John Wiley & Sons, 2010), p.1.
19. Y. Zhang, S.-W. Ng, X. Lu, and Z. Zheng, Chem. Rev. **120**, 2049 (2020). https://doi.org/10.1021/acs.chemrev.9b00483.
20. M. O. Orlandi, *Tin Oxide Materials: Synthesis, Properties, and Applications* (Amsterdam, Netherlands, Elsevier, 2020), p.579.
21. W. L. Butler, J. Opt. Soci. America **52**, 292 (1962). https://doi.org/10.1364/JOSA.52.000292.
22. C. Balocco, L. Mercatelli, N. Azzali, M. Meucci, and G. Grazzini, Sol. Ener. **165**, 199 (2018). https://doi.org/10.1016/j.solener.2018.03.011.
23. M. Chen, S. Cao, K. Xing, Y. Song, X. Han, R. Zeng, B. Zou, and J. Zhao, J. Mater. Chem. C **10**, 9849 (2022). https://doi.org/10.1039/D2TC01963A.
24. A. Khodadadi, M. Farahmandjou, M. Yaghoubi, and A. R. Amani, Int. J. Appl. Ceram. Tech. **16**, 718 (2019). https://doi.org/10.1111/ijac.13065.
25. T. Nestler, S. Fedotov, T. Leisegang, and D. C. Meyer, Critic. Rev. Sol. Stat. Mat. Sci. **44**, 298 (2019). https://doi.org/10.1080/10408436.2018.1490248.

26. H. Mizoguchi and P. M. Woodward, Chem. Mat. **16**, 5233 (2004). https://doi.org/10.1021/cm049249w.
27. M. H. M. Zaid, K. A. Matori, S. H. A. Aziz, H. M. Kamari, Z. A. Wahab, N. Effendy, and I. M. Alibe, J. Non-Crystal. Sol. **449**, 107 (2016). https://doi.org/10.1016/j.jnoncrysol.2016.07.020.
28. A. E. Jiménez-González, J. A. Soto Urueta, and R. Suárez-Parra, J. Cryst. Grow. **192**, 430 (1998). https://doi.org/10.1016/S0022-0248(98)00422-9.
29. S. F. Ahmed, S. Khan, P. K. Ghosh, M. K. Mitra, and K. K. Chattopadhyay, J. Sol-Gel. Sci. Tech. **39**, 241 (2006). https://doi.org/10.1007/s10971-006-7808-x.
30. J. J. Colyn, M.Sc Thesis, University of Alberta, Canada, 2013.
31. N. P. Starling, Eng.D Thesis, University of Surrey, ngland, 2007.
32. D. A. H. Hanaor and C. C. Sorrell, J. Mat. Sci. **46**, 855 (2011). https://doi.org/10.1007/s10853-010-5113-0
33. S. G. Dasari, P. Nagaraju, V. Yelsani, and M. V. Ramana Reddy, J. Mat. Sci. Mat. Elect. **33**, 23447 (2022). https://doi.org/10.1007/s10854-022-09106-8.
34. S. Ghosh, C. Roychaudhuri, R. Bhattacharya, H. Saha, and N. Mukherjee, ACS Appl. Mat. Inter. **6**, 3879 (2014). https://doi.org/10.1021/am404883x.
35. N. Das and P. K. Biswas, J. Mat. Sci. **47**, 289 (2012). https://doi.org/10.1007/s10853-011-5797-9.
36. A. Bhakar, M. Taxak, and S. K. Rai, J. Appl. Cryst. **56**, 1466 (2023). https://doi.org/10.1107/S1600576723007367.
37. C. Mrabet, A. Boukhachem, M. Amlouk, and T. Manoubi, J. All. Comp. **666**, 392 (2016). https://doi.org/10.1016/j.jallcom.2016.01.104 .
38. F. A. Denis, P. Hanarp, D. S. Sutherland, J. Gold, C. Mustin, P. G. Rouxhet, and Y. F. Dufrêne, Langmuir **18**, 819 (2002). https://doi.org/10.1021/la011011o.
39. A. Z. Noor, S. Bibi, M. Asrar, M. Imran, S. Afzal, S. Abdal, and M. Atif, RSC Adv. **14**, 35727 (2024). https://doi.org/10.1039/D4RA06342B.

تحضير أفلام $AlCl_3$:ITO باستخدام طريقة طلاء السول جل

الاء مصطفى ذيبان[1] وفلاح حسن علي[1]

[1] قسم الفيزياء، كلية العلوم، جامعة بغداد، بغداد، العراق

الخلاصة

استخدمت هذه الدراسة طريقة التغطيس بالغمس باستخدام طريقة سول-جل لإنتاج أغشية رقيقة من أكسيد الإنديوم والقصدير النقي (ITO) وأغشية رقيقة من ITO مطعمة بكلوريد الألومنيوم ($AlCl_3$) بتراكيز مختلفة (50، 100، و150% وزناً). استُخدمت مواد أولية مثل كلوريد الإنديوم ($InCl_3$) وكلوريد القصدير ($SnCl_4$) في عملية التخليق. خضعت عينات ITO المُصنّعة لتحليل دقيق باستخدام تقنيات الأشعة فوق البنفسجية والمرئية، ومجهر القوة الذرية (AFM)، وحيود الأشعة السينية (XRD)، ومجهر المسح الإلكتروني ذي الانبعاث الميداني/مطيافية تشتت طاقة الأشعة السينية (FE-SEM/EDX)، ومطيافية تحويل فورييه للأشعة تحت الحمراء (FTIR). كشف تحليل XRD عن وجود قمة قوية للمستوى (222)، مما يدل على أن أكسيد الإنديوم في الأغشية الرقيقة منظم بشكل جيد للغاية. أكد تحليل EDX وجود عناصر، بما في ذلك الإنديوم (In)، والأكسجين (O)، والقصدير (Sn)، والألومنيوم (Al)، والكلور (Cl)، ضمن الطبقات المترسبة. وفقًا لصور المجهر الإلكتروني الماسح ذي الانبعاث الميداني (FE-SEM)، بلغ متوسط أقطار الجسيمات 45.47 نانومترًا لطبقة أكسيد الإنديوم والقصدير النقية (ITO)، و62.48 و42.72 و35.25 نانومترًا لطبقات ITO الممزوجة بنسب 50 و100 و150% وزنيًا من كلوريد الألومنيوم ($AlCl_3$) على التوالي. وأشار تحليل المجهر الذري الماسح (AFM) إلى أن متوسط حجم الجسيمات في طبقة ITO النقية يبلغ 61 نانومترًا. في المقابل، بلغ متوسط حجم الجسيمات في الطبقات الممزوجة بـ AlCl3 بنسب 50 و100 و150% وزنيًا 17 و21 و68 نانومترًا على التوالي. بالإضافة إلى ذلك، تم قياس فجوة النطاق البصري لطبقة ITO عند 4.5 إلكترون فولت. أما بالنسبة للطبقات الممزوجة بـ AlCl3 بنسب 50 و100 و150% وزنيًا، فقد وُجد أن فجوات الطاقة تبلغ 1.5 و1.73 و1.83 إلكترون فولت على التوالي. كانت زاوية التلامس المقاسة لفيلم ITO هي 332.57 درجة؛ أما تلك التي تم قياسها باستخدام AlCl3 عند 50 و100 و150٪ فكانت 65.39 درجة و85.99 درجة و78.12 درجة على التوالي.

الكلمات المفتاحية: أغشية $AlCl_3$، طريقة الطلاء بالغمس على شكل سول-جل، أكسيد القصدير الإنديوم (ITO)، الخواص البصرية، زاوية التلامس.